Assessment of CO_2 Injection in Fractured Calcite Rock Clogged by *Pseudomonas putida* Biofilm

Varvara Sygouni[1], Georgios C. Dimadis[2] and Constantinos V. Chrysikopoulos[3,*]

[1]*Department of Civil Engineering, University of Patras, 26500 Patras, Greece;* [2]*School of Civil Engineering, Aristotle University of Thessaloniki, 54124 Thessaloniki, Greece and* [3]*School of Environmental Engineering, Technical University of Crete, 73100 Chania, Greece*

Abstract: The effect of a possible accidental carbon dioxide (CO_2) leakage from deep geologic storage reservoirs on shallow subsurface sources of potable water is receiving considerable attention, because groundwater quality can be compromised. In this work, the effect of a gas CO_2 leakage on the permeability of a fractured calcite rock bioclogged with *Pseudomonas (P.) putida* biofilm was investigated experimentally under ambient conditions. Initially, a batch experiment of *P. putida* inactivation in the presence and absence of calcite was performed. Subsequently, *P. putida* biofilm was developed in a fractured calcite rock from Mons, Belgium. The fractured rock permeability was measured before and after bioclogging, as well as after CO_2 injection. The experimental results indicated that calcite can enhance *P. putida* growth, and that a *P. putida* biofilm formation can practically eliminate fractured rock permeability (99% reduction). However, sudden CO_2 injection increased the permeability of the bioclogged fractured calcite rock, but only to a level substantially lower than that corresponding to the initial permeability of the clean fractured rock.

Keywords: Biofilm, *P. putida*, CO_2, Calcite rock, Permeability.

1. INTRODUCTION

Storage of carbon dioxide (CO_2) in deep geologic formations is a promising solution for the reduction of greenhouse gases from the atmosphere. However, possible accidental leakage of CO_2 could degrade the water quality of overlying shallow aquifers [1-5]. Although numerous studies published in the literature have focused on the impact of pH decrease associated with CO_2 leakage on mobilization of naturally occurring hazardous trace metals and ions in aquifers due to processes involving desorption and dissolution [1,6,7], the effect of CO_2 leakage on bacteria and biofilms in shallow overlying aquifers has received very little attention [8-10].

A biofilm consists mainly of three-dimensional structures of bacterial cells and extracellular polymeric substance (EPS). Growth of biofilms in porous media (e.g. soil, rocks, membranes) results in permeability reduction and clogging [11]. The pore clogging of porous media by biofilms is known as "bioclogging" [8,12,13]. Although there are numerous cases where bioclogging has detrimental consequences, such as progressive plugging of water wells, ponds and trenches used for artificial aquifer recharge [14], or wetland wastewater treatment [15-17], there are several instances where bacteria and bioclogging may be used to advantage. Bacteria are known to enhance oil recovery [18,19]. Biofilms are also used as barriers in porous media and landfills [20,21], in bioremediation enhancement [22,23], prevention of well bore CO_2 leakage [24], and geologic containment CO_2 leakage [25-27].

In this work, the effect of sudden accidental leakage of CO_2 in a bioclogged fractured calcite rock was investigated. Certainly, the short-term effects of CO_2 on bacteria and biofilms within a freshwater aquifer are not sufficiently understood. To our knowledge, the response of bacteria and biofilms within a bioclogged fractured aquifer to CO_2 leakage has not been previously explored.

2. MATERIALS AND METHODS

2.1. Calcite Fractured Core Samples

Chalk from Mons, Belgium was used in this study. The morphology of the chalk rock was captured with a scanning electron microscopy (SEM) system JEOL (JSM 84A). A SEM image of the chalk rock is shown in Figure **1**. The elemental composition of the chalk rock was determined by dissolving 200 mg of the solid rock into 6 mL HCl 37% and 1 mL HF 40%, followed by a microwave oven digestion procedure (Berghof speedwave 2), and atomic absorption spectroscopy (Shimadzu AA6300). The various elements of the chalk are listed in Table **1**. Clearly, this is high purity chalk, because it consists of >98% calcite (see Table **1**). The effective porosity, θ_e [-] (volume of connected voids to total volume), of the intact chalk was determined gravimetrically equal to θ=39.5%. The intrinsic permeability, k [Da], of the intact chalk was determined as k=1.6 mDa

*Address correspondence to this author at the School of Environmental Engineering, Technical University of Crete, 73100 Chania, Greece; Tel: (+30) 28210-37797; E-mail: cvc@enveng.tuc.gr

(where Da=darcy=10^{-12} m^2) from Darcy's law with experimental data of pressure drop versus volumetric flow rate collected by placing a cylindrical chalk sample in a core holder (QRC-series, Vinci technologies) where the confining pressure was applied by a hand oil press, constant inlet pressure was applied by a high precision volume/pressure controller (GDS instruments), constant outlet pressure was controlled by a back-pressure-regulator (BPR Vinci technologies), the penetrating fluid was distilled water, and the resulting volumetric flow rate was estimated by effluent volume determination.

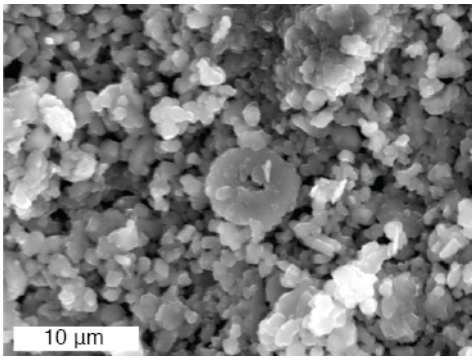

Figure 1: SEM image of the chalk rock.

Table 1: Elemental Composition of Chalk Rock

Element	C (ppm)	C (%)
Ca	404908	98.64
Mg	1577	0.38
K	326	0.08
Na	516	0.13
Fe	558	0.14
Al	993	0.24
Si	1584	0.39
Cd	0.38	0.00
Cr	4.21	0.00
Cu	2.17	0.00
Ni	17.64	0.00
Pb	0.45	0.00
Zn	10.82	0.00

Four cylindrical core samples were extracted from the chalk rock. Wet core drilling was performed with a sandstone driller (Milwaukee 4096-4, 2.8 kW) with 1.5-inch (3.8 cm) core drill bit, operated at 450 rpm. A fracture was induced at the long axis of each core sample by dynamic impact, imposed with a set of parallel custom-made metallic jaws (see Figures **2a,b**). Samples A and B were fractured dry, whereas as samples Γ and Δ were fractured after water saturation. However, only the core sample Δ, with length L=13 cm and diameter d=3.8 cm, was used in this study.

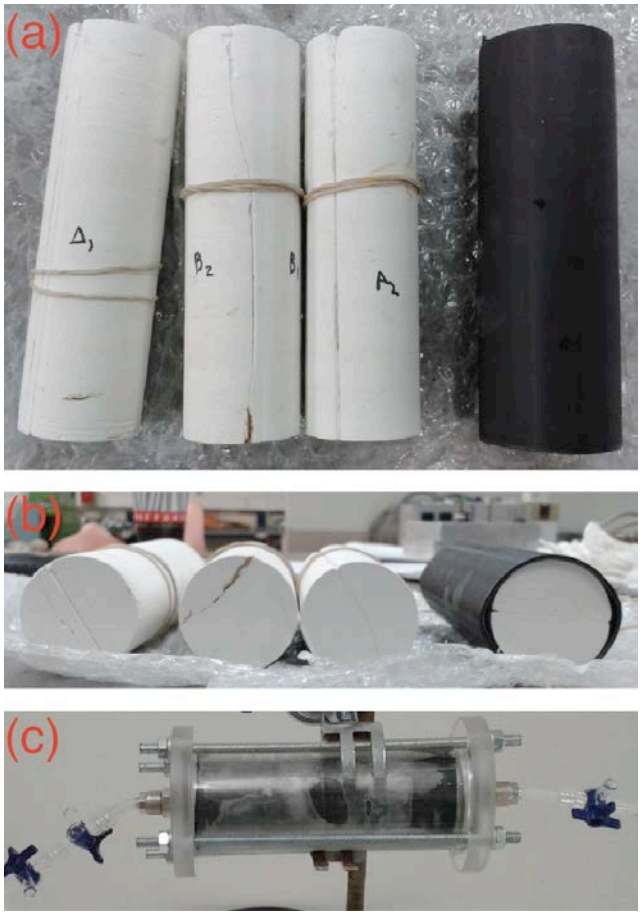

Figure 2: Pictures of the cylindrical fractured core samples A, B, Γ, and Δ, exhibiting: (**a**) the long main core axes, one core sample is placed within a heat shrinkable Teflon® tube, (**b**) the cylindrical faces of the cores, and (**c**) core sample Δ with shrunk tube mounted inside a Plexiglass® cylindrical column.

A picture of the two halves of core sample Δ (indicated as sections Δ1 and Δ2) is presented in Figure **3a**. A three-dimensional laser scan (3D Scanner UltraHD NextEngine) was used to characterize the roughness of the fracture surfaces of specimen sections Δ1 and Δ2. Elevation counter plots of the surfaces Δ1 and Δ2 are shown in Figure **3b**, whereas the corresponding long axis profiles, taken every 4 mm, are shown in Figure **3c**.

In order to characterize the fracture surface type of core sample Δ, the Joint Roughness Coefficient (JRC) introduced by Barton and Choubey [28] must be determined. In this study, numeric data from the 3D scan were used for more precise evaluation of JRC by the following corelation [29]:

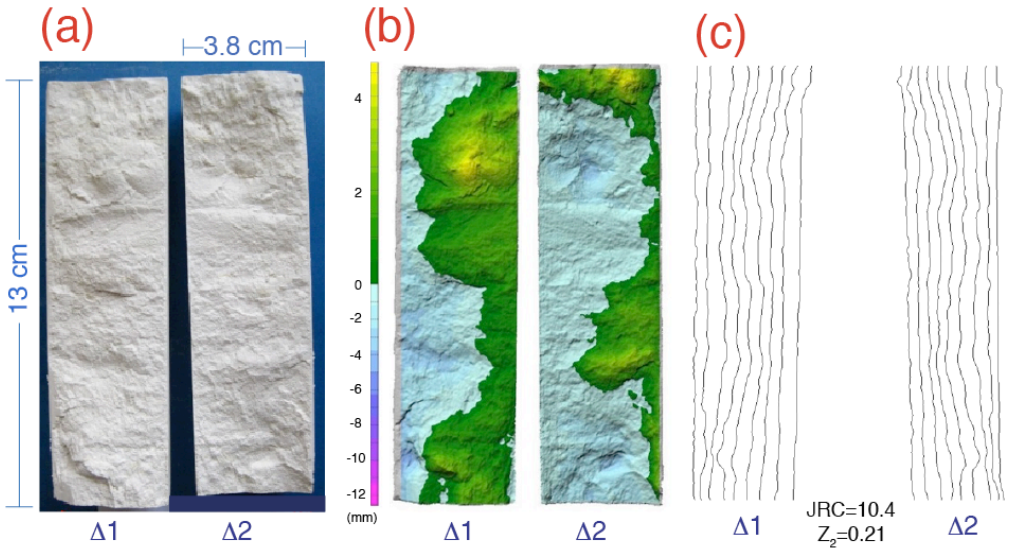

Figure 3: Core sample Δ, (**a**) photo of core sample halves Δ1 and Δ2, (**b**) elevation counter plot, and (**c**) long axis profiles taken every 4 mm.

$$JRC = 32.69 + 32.98 \log_{10} Z_2 \quad (1)$$

where Z_2 is the root mean square of the first derivative of the long axis profile, which is expressed in a discrete form as follows [29,30]:

$$Z_2 = \left[\frac{1}{m(\Delta x)^2} \sum_{i=1}^{m} \left(y_{i+1} - y_i \right) \right]^{1/2} \quad (2)$$

where m is the number of sampling intervals, Δx is the sampling interval length, $(y_{i+1}-y_i)$ is the difference between two adjacent sampling points. Employing equation (2) with Δx=1 mm, to each one of the 9 long axis profiles (axis interval 4 mm) of core section Δ1 (see Figure **3c**), the average value of coefficient Z_2 was calculated equal to Z_2=0.21. Also, in view of equation (1), the corresponding value of JRC was calculated equal to JRC=10.4. Therefore, based on the standard roughness profiles, the fractured rock sample Δ can be characterized as smooth undulating joint [31].

To jacket the core sample Δ, a heat shrinkable Teflon® tube (see Figure **2a**), was used, which was shrunk over the core, and then mounted rigidly inside a Plexiglass® cylinder. A cap was firmly placed on each side of the Plexiglass® cylinder. Furthermore, a hole was opened on the center of each cap, which were used as fluid inlet and outlet ports (see Figure **2c**).

2.2. Intrinsic Permeability of Fractured Core

Based on Darcy's law, the intrinsic permeability, k [L^2], is defined as follows [32]:

$$Q = -\frac{kA}{\mu}\frac{\Delta P}{L} \Rightarrow k = -\mu \frac{L}{A}\left(\frac{Q}{\Delta P}\right) \quad (3)$$

where Q [L^3/t] is the volumetric flow rate, $A=\pi d^2$ [L^2] is the cross-sectional area to flow, ΔP [$M/(t^2 \cdot L)$] is the hydraulic pressure drop, μ [$M/(t \cdot L)$] is the fluid viscosity, and L [L] is the length of the core sample. For the estimation of the intrinsic permeability of the fractured core sample Δ, several hydraulic pressure drops:

$$\Delta P = \rho g \Delta h \quad (4)$$

where ρ [M/L^3] is the fluid density, g=9.81 m/s^2 is the acceleration due to gravity, and Δh [L] is the hydraulic head drop, were applied across the Plexiglass® cylinder by varying Δh. The corresponding volumetric flow rates, were determined using the following expression:

$$Q = \frac{\Delta V}{\Delta t} \quad (5)$$

where ΔV [L^3] is the fluid volume passing through the fractured core sample over a preselected time interval Δt [t]. Subsequently, a plot of ΔP versus Q values was constructed and the slope, of the linear regression line, which is proportional to k, was determined. Given that the fractured rock sample Δ has length L=13 cm and diameter d=3.8 cm, the corresponding intrinsic permeability was determined to be equal to k=3.89 Da. An illustration of the experimental set up employed in this study is shown in Figure **4**. Note that by moving vertically the constant head reservoir a desired value of Δh can be obtained.

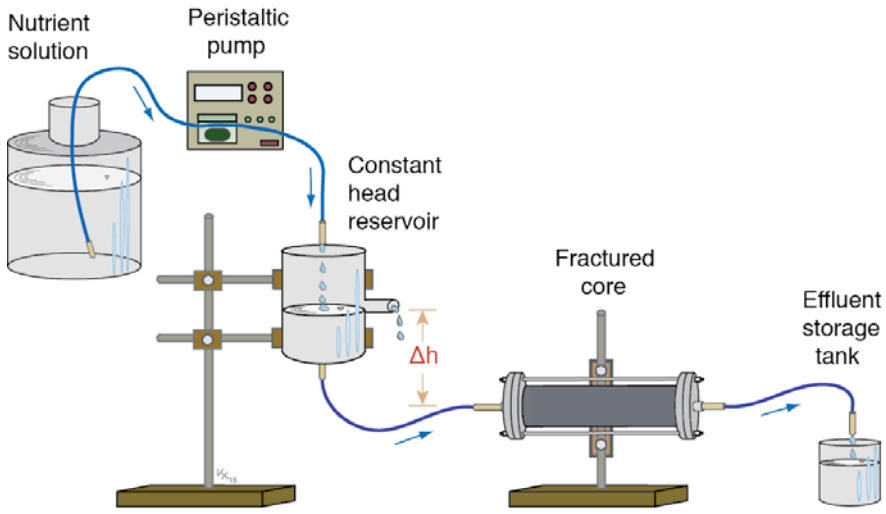

Figure 4: Schematic illustration of the experimental setup.

2.3. Bacteria and Biofilm

The biofilm within the fractured rock was grown with *P. putida*, which was cultured by following well-established procedures [33,34]. Briefly, *P. putida* was cultured in 10 mL of nutrient broth (Laury Pepto Bios Broth 35.6 g/L, Biolife Italiana Srl, with typical composition as listed in Table **2**) for 20 hr at 30 °C in an orbital shaker (Innova 43, New Brunswick Scientific, NJ) at 140 rpm. A culture volume of 5 mL was transferred in 250 mL of the nutrient broth and it was re-cultured for 20 hr at 30 °C and 140 rpm. Finally, bacteria were collected by centrifugation for 8 min at 10000 rpm (SL40R, Thermo Scientific), washed out several times with distilled deionized water and subsequently, washed out once more with sterile saline before they were stored in sterile saline at 4 °C. Prior to injection of the culture into the fractured rock, *P. putida* cells were diluted in nutrient broth to the desired concentration of approximately 10^8 cfu/mL.

Table 2: Nutrient Broth Composition

Compound	C (g/L)
Tryptone ($C_4H_{11}NO_3$·HCl)	20
Lactose ($C_{12}H_{22}O_{11}$)	5
Sodium chloride (NaCl)	5
Sodium-lauryl-sulfate ($C_{12}H_{26}$·$NaSO_4$)	0.1
Dipotassium-hydrogen-phosphate (K_2HPO_4)	2.75

The concentration of *P. putida* in the effluent fractured rock was measured using the spread plate method as outlined by Sygouni et al. [10]. Briefly, aliquots of 0.1 mL were inoculated on petri dishes containing sterile Agar (Lab-Agar™ PS 133, with typical composition as listed in Table **3**). The colonies were measured after incubation of petri dishes in an incubator chamber (GCA Corporation/Precision Scientific Group, IL) at 37 °C for 48 h. A typical petri dish after incubation is shown in Figure **5**.

Table 3: Lab-Agar™ PS 133 Composition

Compound	C (g/L)
Pancreatic digest of gelatin	20.0
Magnesium chloride ($MgCl_2$)	1.4
Potassium sulfate (K_2SO_4)	1.0
Cetrimide ($C_{17}H_{38}BrN$)	0.3
Agar	13.6

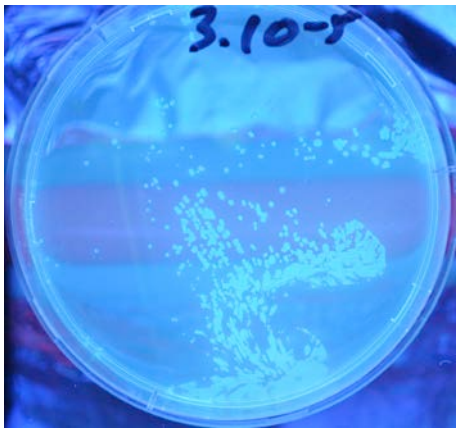

Figure 5: A petri dish over fluorescent lighting, containing *P. putida* colonies after incubation of a 50-fold (5-orders of magnitude) diluted core effluent liquid sample.

3. EXPERIMENTAL RESULTS AND DISCUSSION

3.1. CO_2 Injection in Bio-Clogged Fractured Core

In order to investigate the effect of calcite on *P. putida* culture, a set of relatively simple batch experiments were performed. In one test tube, 10 mL of *P. putida* culture were mixed with 10 mL nutrient, whereas in a second test tube, 10 mL of *P. putida* culture were mixed with 10 mL nutrient and 100 mg/L calcite. The *P. putida* concentration, C [cfu], in both test tubes was measured over a time period of 6 days. The experimental data were normalized with respect to the initial *P. putida* concentration, $C_o=2\times10^5$ cfu, and presented graphically in Figure **6**. The experimental data indicate that the normalized *P. putida* concentration increases in the presence of calcite (see Figure **6**). This observation can be explained by the fact that *P. putida* is known to biosynthesize tryptophan ($C_{11}H_{12}N_2O_2$), which is an aromatic amino acid [35]. Furthermore, it has been reported in the literature that tryptophan biosynthesis by *P. putida* is enhanced in the presence of calcite [36]. Note that the *P. putida* nutrient contains tryptone ($C_4H_{11}NO_3{\cdot}HCl$) (see Table **2**), which is rich in tryptophan. Also, some bacteria may use tryptophan as a source of carbon and energy. This result is in agreement with other findings published in the literature suggesting that calcium enhances *P. putida* biofilm formation [37]. During the development of *P. Putida* biofilms, protein LapF is instrumental in *P. Putida* biofilm maturation; whereas, calcium cations aggregate the LapF protein and enhance interactions of bacteria, which promote biofilm development [37]. It is worthy to note that after 6 days, the concentration of *P. putida* in both tubes was reduced to approximately equal levels.

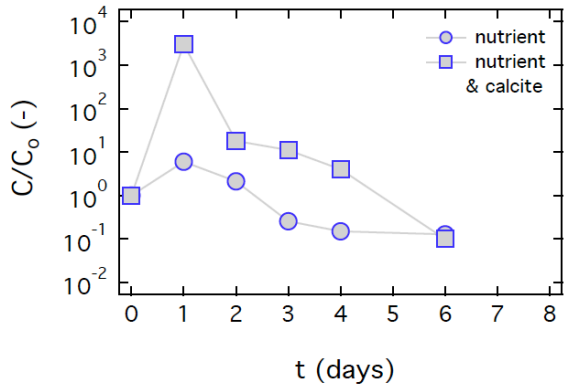

Figure 6: Normalized *P. putida* concentration measured over a 6-day time period in the presence of nutrient (circles), and nutrient as well as calcite (squares).

In order to investigate the impact of CO_2 leakage in a fractured calcite rock bioclogged with biofilm, a *P. putida* solution was injected into the jacketed core sample Δ. The injection of nutrient broth was initiated approximately 3 hours later. This 3-hour delay period was essential for the bacteria to attach onto the fracture surfaces. The nutrient solution was injected under constant pressure drop with a flow rate of Q=0.69 mL/h (see Figure **4**). The effluent volume of nutrient and the effluent *P. putida* concentration were measured periodically. When the fractured core sample Δ was practically bio-clogged due to the formation of *P. putida* biofilm, the intrinsic permeability of the core sample Δ was determined. Next, CO_2 was injected into the jacketed core sample Δ for 20 min with constant flow rate of 0.51 L/min. One day after the CO_2 injection, the intrinsic permeability of core sample Δ was re-determined.

The effluent mean volumetric flow rate (Q [mL/h]) as a function of time is presented in Figure **7**. The experimental data suggest that after approximately 20 days, the fractured core sample Δ was practically bioclogged by the formation of *P. putida* biofilm, because the effluent Q was essentially diminished.

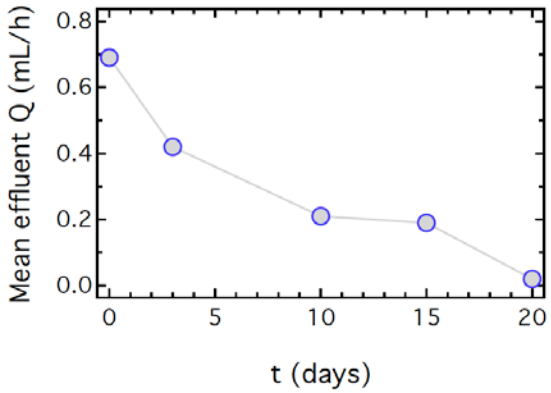

Figure 7: Fluid effluent volume from the fractured core sample versus time.

The effluent *P. putida* concentration experimental data are presented in Figure **8**. Note that the effluent *P. putida* concentration progressively increased. This concentration increase contributed to the progressive biofilm formation increase within the fractured core. Note that CO_2 breakthrough was observed after 16 minutes of CO_2 injection. Also, during the CO_2 injection the effluent *P. putida* concentration was reduced by approximately two-orders of magnitude (see the square symbol in Figure **8**). Furthermore, the effluent *P. putida* concentration was additionally reduced by one-order of magnitude the day after the CO_2 injection (see the diamond symbol in Figure **8**). This reduction in *P. putida* concentration is attributed to the biofilm mass reduction, caused by the sudden CO_2 injection. Also,

the CO_2 injection resulted in effluent pH reduction. Note that before CO_2 injection, the effluent pH was equal to pH=7.2, whereas at the end of CO_2 injection it was reduced to pH=6.9. This is an expected result, because CO_2 reacts with water to form carbonic acid (H_2CO_3), which dissociates to bicarbonate (HCO_3^-) and hydrogen ions (H^+), and in turn HCO_3^- dissociates to carbonate (CO_3^{2-}) and H^+ [38].

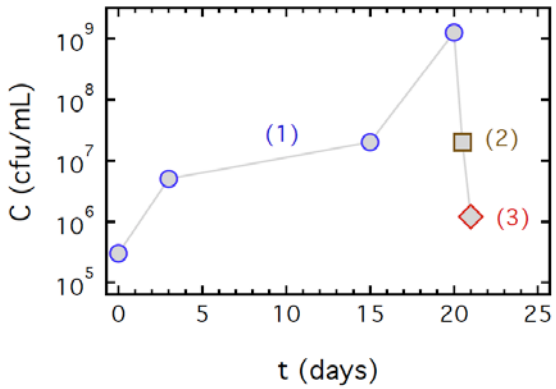

Figure 8: Concentration of *P. putida* at the outlet of the fractured core sample as a function of time collected: (1) during biofilm growth (circles), (2) during CO_2 injection (square), and (3) one day after the CO_2 injection (diamond).

The intrinsic permeability of core sample Δ was determined at three different times: (i) during the initial stage, before the injection of bacteria into the clean fractured core, (ii) at the end of fracture bioclogging stage, prior to CO_2 injection, and (iii) during the final stage, one day after the completion of CO_2 injection. The measured pressure drops across the fractured core sample Δ versus nutrient flow rate, before and after CO_2 injection, are shown in Figure **9**. The corresponding intrinsic permeability values of the fractured rock were determined from the slopes of the three fitted lines presented in Figure **9**. The resulting intrinsic permeability values are listed in Table **4**. The day after the completion of CO_2 injection, the intrinsic permeability of the fractured rock (k=1.95 Da) was only one-half of its initial value (k=3.90 Da), because several sections of the biofilm formation within the fractured rock were not fully penetrated by CO_2. The intrinsic permeability of the fractured rock measured at the end of the fracture bioclogging stage (k=0.04 Da), suggested that under the experimental conditions of this study, the *P. putida* biofilm did not seal completely every single void space within the fractured rock, and thus did not yield a perfectly impermeable barrier. However, additional parametric analyses are needed in order to fully understand the impact of CO_2 flow rate on *P. putida* biofilm breakdown, in conjunction with biofilm age. Older biofilm (fully developed biofilm) is expected to be more resistant to breakdown due to CO_2 releases.

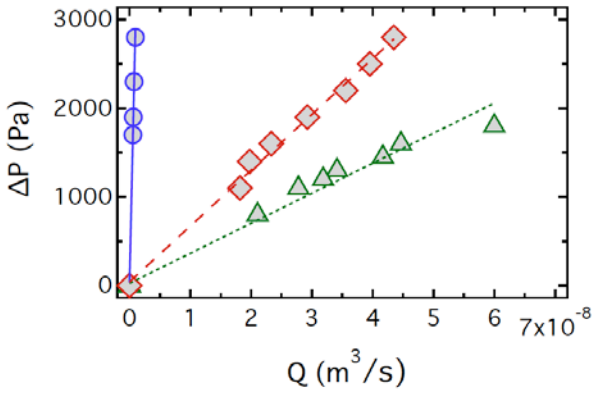

Figure 9: Pressure drop across the fractured core sample Δ as a function of volumetric flow rate, measured: (1) before bacteria injection (triangles), (2) before CO_2 injection into the bioclogged fractured core (circles), and (3) after CO_2 injection (diamonds). The straight lines are linear regression lines, with slopes proportional to the corresponding intrinsic permeability values.

Table 4: Estimated Intrinsic Permeability of the Fractured Rock Sample Δ

Experimental Stage	k (Da)
Initial stage (clean fracture)	3.90
End of fracture bioclogging stage (prior to CO_2 injection)	0.04
Final stage (after CO_2 injection)	1.95

4. SUMMARY AND CONCLUSIONS

In this work the impact of CO_2 leakage in a bioclogged fractured calcite rock was investigated experimentally. It was shown that calcite contributed to the growth of *P. putida*. Furthermore, under the experimental conditions of this study, *P. putida* biofilm growth was severely reduced. However, the fractured rock permeability was not eliminated completely. Just after the completion of a sudden CO_2 release, the fractured rock permeability was shown to increase to one-half the permeability of the perfectly clean fractured rock (original permeability). Clearly, the *P. putida* biofilm is significantly affected by CO_2 releases. Consequently, *P. putida* biofilm development can not be recommended as an efficient method for sealing shallow potable water aquifers from underlying leaking geologic storage reservoirs. Although the results from this study have improved our understanding of the impact of CO_2 sudden release on *P. putida* biofilm within a fractured calcite rock, several questions concerning the long-

term effects of continuous CO_2 releases on biofilm growth still have to be addressed.

NOMENCLATURE

C	=	concentration of *P. putida* (cfu), ML^{-3}
C_o	=	initial *P. putida* concentration (cfu), ML^{-3}
d	=	core sample diameter, L
g	=	acceleration due to gravity, Lt^{-2}
h	=	hydraulic head, L
k	=	intrinsic permeability, L^2
L	=	length of core sample, L
m	=	number of sampling intervals, (-)
Q	=	volumetric flow rate, L^3t^{-1}
V	=	fluid volume, L^3
y_{i+1}-y_i	=	difference between two adjacent sampling points, L
ΔP	=	pressure drop (Pa), $Mt^{-2}L^{-1}$
Δt	=	time interval, t
Δx	=	sampling interval length, L
θ_e	=	effective porosity, (-)
μ	=	fluid viscosity (Pa s), $Mt^{-1}L^{-1}$
ρ	=	fluid density, ML^{-3}

ABBREVIATIONS

cfu	=	Colonies forming units
EPS	=	Extracellular polymeric substance
JRC	=	Joint roughness coefficient
SEM	=	Scanning electron microscopy

ACKNOWLEDGEMENT

This research has been co-financed by the European Union (European Social Fund-ESF) and Greek National Funds through the Operational program "Education and Lifelong Learning" under the action Thales (Project: GEOMECS). The authors are thankful to L. Papadopoulou for recording the SEM image, C. Georgiadis, for conducting the 3D scanning of the specimens, and C. Kanellopoulos for the elemental composition analysis of the rock.

REFERENCES

[1] Wang S, Jaffe PR. Dissolution of a mineral phase in potable aquifers due to CO_2 releases from deep formations; effect of dissolution kinetics. Energy Convers Manage. 2004; 45: 2833-2848.
http://dx.doi.org/10.1016/j.enconman.2004.01.002

[2] Keating E, Fessenden J, Kanjorski N, Koning D, Pawar R. The impact of CO_2 on shallow groundwater chemistry: observations at a natural analog site and implications for carbon sequestration. Environ Earth Sci. 2010; 60: 521-536.
http://dx.doi.org/10.1007/s12665-009-0192-4

[3] Kharaka YK, Thordsen JJ, Kakouros E, Ambats G, Herkelrath WN, Beers SR, *et al*. Changes in the chemistry of shallow groundwater related to the 2008 injection of CO_2 at the ZERT field site, Bozeman, Montana. Environ Earth Sci. 2010; 60(2): 273-284.
http://dx.doi.org/10.1007/s12665-009-0401-1

[4] Lu J, Partin J, Hovorka S, Wong C. Potential risks to freshwater resources as a result of leakage from CO2 geological storage: a batch-reaction experiment. Environ Earth Sci. 2010; 60(2): 335-348.
http://dx.doi.org/10.1007/s12665-009-0382-0

[5] Zheng L, Apps JA, Spycher N, Birkholzer JT, Kharaka YK, Thordsen JJ, *et al*. Geochemical modeling of changes in shallow groundwater chemistry observed during the MSU-ZERT CO_2 injection experiment. Int J Greenhouse Gas Control 2012; 7: 202-217.
http://dx.doi.org/10.1016/j.ijggc.2011.10.003

[6] Zheng L, Apps JA, Zhang Y, Xu T, Birkholzer JT. On mobilezation of lead and arsenic in groundwater in response to CO_2 leakage from deep geological storage. Chem Geol 2009; 268: 281-297.
http://dx.doi.org/10.1016/j.chemgeo.2009.09.007

[7] Montes-Hernandez G, Renard F, Lafay R. Experimental assessment of CO_2-mineral-toxic ion interactions in a simplified freshwater aquifer: implications foe CO_2 leakage from deep geological storage. Environ Sci Technol. 2013; 47: 6247-6253.
http://dx.doi.org/10.1021/es3053448

[8] Thullner M, Zeyer J, Kinzelbach W. Influence of microbial growth on hydraulic properties of pore networks. Transp Porous Media 2002; 49: 99-122.
http://dx.doi.org/10.1023/A:1016030112089

[9] Kirk MF, Santillan EFU, McGrath LK, Altman SJ. Variation in hydraulic conductivity with decreasing pH in a biologically-clogged porous medium. Int J Greenhouse Gas Control 2012; 11: 133-140.
http://dx.doi.org/10.1016/j.ijggc.2012.08.003

[10] Sygouni V, Manariotis ID, Chrysikopoulos CV. Experimental investigation of the effect of carbon dioxide on *Pseudomonas putida* biofilms in a two-dimensional glass network model. Inter J Greenhouse Gas Control 2015; submitted.

[11] Taylor S, Jaffe PR. Biofilm growth and the related changes in the physical properties of a porous medium 1: experimental investigation. Water Resour Res 1990; 26(9): 2153-2159.

[12] Mack WN, Mack JP, Ackerson AO. Microbial film development in a trickling filter. Microbial Ecol. 1975; 2: 215-226.
http://dx.doi.org/10.1007/BF02010441

[13] Glatstein DA, Francisca FM. Hydraulic conductivity of compacted soils controlled by microbial activity. Environ Technol. 2014; 35(15): 1886-1892.
http://dx.doi.org/10.1080/09593330.2014.885583

[14] Baveye P, Vandevivere P, Hoyle BL, DeLeo PC, de Lozada DS. Environmental impact and mechanisms of the biological

clogging of saturated soils and aquifer materials. Crit Rev Environ Sci Technol. 1998; 28(2): 123-191.

http://dx.doi.org/10.1080/10643389891254197

[15] Langergraber G, Haberl R, Laber J, Pressl G. Evaluation of substrate clogging processes in vertical flow constructed wetlands. Water Sci Technol 2003; 48(5): 25-34.

[16] Nivala J, Knowles P, Dotro G, Garcıa J, Wallace S. Clogging in subsurface-flow treatment wetlands: Measurement, modeling and management. Water Res. 2012; 46: 1625-1640.

http://dx.doi.org/10.1016/j.watres.2011.12.051

[17] Hua G, Zeng Y, Zhao Z, Cheng K, Chen G. Applying a resting operation to alleviate bioclogging in vertical flow constructed wetlands: An experimental lab evaluation. J Environ Manag. 2014; 136: 47-53.

http://dx.doi.org/10.1016/j.jenvman.2014.01.030

[18] Soudmand-asli A, Ayatollahi SS, Mohabatkar H, Zareie M, Shariatpanahi SF. The *in situ* microbial enhanced oil recovery in fractured porous media. J Petrol Sci Eng. 2007; 58: 161-172.

http://dx.doi.org/10.1016/j.petrol.2006.12.004

[19] Sen R. Biotechnology in petroleum recovery: The microbial EOR. Progr Energy Combustion Sci. 2008; 34(6): 714-724.

http://dx.doi.org/10.1016/j.pecs.2008.05.001

[20] Seki K, Miyazaki T, Nakano M. Effects of microorganisms on hydraulic conductivity decrease in infiltration. Eur J Soil Sci. 1998; 49(2): 231-236.

http://dx.doi.org/10.1046/j.1365-2389.1998.00152.x

[21] Kanmani S, Gandhimathi R, Muthukkumaran K. Bioclogging in porous media: influence in reduction of hydraulic conductivity and organic contaminants during synthetic leachate permeation. J Environ Health Sci Eng. 2014; 12(1): 126.

http://dx.doi.org/10.1186/s40201-014-0126-2

[22] James GA, Warwood BK, Hiebert R, Cunningham AB. Microbial barriers to the spread of pollution. In Bioremediation (ed. JJ Valdes), pp. 1–14. Amsterdam, the Netherlands: Kluwer Academic (2000).

http://dx.doi.org/10.1007/978-94-015-9425-7_1

[23] Cunningham AB, Sharp RR, Hiebert R, Garth J. Subsurface biofilm barriers for the containment and remediation of contaminated groundwater. Bioremediation J. 2003; 7(3): 151-164.

http://dx.doi.org/10.1080/713607982

[24] Cunningham AB, Gerlach R, Spangler L, Mitchell AC, Parks S, Phillips A. Reducing the risk of well bore leakage of CO_2 using engineered biomineralization barriers. Energy Procedia 2011; 4: 5178-5185.

http://dx.doi.org/10.1016/j.egypro.2011.02.495

[25] Cunningham AB, Gerlach R, Spangler L, Mitchell AC, Microbial Enhanced Geologic containment of sequestered supercritical CO_2. Energy Procedia 2009; 1: 3245-3252.

http://dx.doi.org/10.1016/j.egypro.2009.02.109

[26] Mitchell AC, Phillips A, Hiebert R, Cunningham AB. Biofilm enhanced subsurface sequestration of supercritical CO_2. Int J Greenhouse Gas Control 2009; 3(1): 90-99.

http://dx.doi.org/10.1016/j.ijggc.2008.05.002

[27] Phillips AJ, Lauchnor E, Eldring J, Esposito R, Mitchell AC, Gerlach R, *et al*. Potential CO_2 leakage reduction through biofilm-induced calcium carbonate precipitation. Env Sci Technol. 2012; 47: 142-149.

http://dx.doi.org/10.1021/es301294q

[28] Barton N, Choubey V. The shear strength of rock joints in theory and practice. Rock Mech Felsmechanik Mecanique Des Roches 1977; 10(1-2): 1-54.

http://dx.doi.org/10.1007/BF01261801

[29] Yang ZY, Lo SC, Di CC. Reassessing the joint roughness coefficient (JRC) estimation using Z2. Rock Mech Rock Eng. 2001; 34(3): 243-251.

http://dx.doi.org/10.1007/s006030170012

[30] Myers NO. Characterization of surface roughness. Wear 1962; 5(3): 182-189.

http://dx.doi.org/10.1016/0043-1648(62)90002-9

[31] Du S, Hu Y, Hu X. Generalized models for rock joint surface shapes. Scientific World J. 2014; 2014: 171873.

http://dx.doi.org/10.1155/2014/171873

[32] Bear J. Dynamics of Fluids in Porous Media, Dover (1972).

[33] Vasiliadou IA, Chrysikopoulos CV. Cotransport of *Pseudomonas putida* and kaolinite particles through water-saturated columns packed with glass beads. Water Resour Res. 2011; 47: W02543.

http://dx.doi.org/10.1029/2010WR009560

[34] Chrysikopoulos CV, Syngouna VI, Vasiliadou IA, Katzourakis VE. Transport of *Pseudomonas putida* in a three-dimensional bench scale experimental aquifer. Transp Porous Media 2012; 94: 617-642.

http://dx.doi.org/10.1007/s11242-012-0015-z

[35] Pasupuleti M, Chalupka A, Mörgelin M, Schmidtchen A, Malmsten M. Tryptophan end-tagging of antimicrobial peptides for increased potency against *Pseudomonas aeruginosa*. Biochim Biophys Acta 2009; 1790(8): 800-808.

http://dx.doi.org/10.1016/j.bbagen.2009.03.029

[36] Al-Zahrani NHM. Improving ability of *Pseudomonas putida* strain to biosynthesis of L-tryptophan. Life Sci J. 2014; 11: 476-481.

[37] Martinez-Gil M, Romero D, Kolter R, Espinosa-Urgela M. Calcium causes multimerization of the large adhesin LapF and modulates biofilm formation by *Pseudomonas putida*. J Bacteriol. 2012; 194(24): 6782-6789.

http://dx.doi.org/10.1128/JB.01094-12

[38] Stumm W, Morgan JJ. Aquatic Chemistry, An Introduction Emphasizing Chemical Equilibria in Natural Waters, 2nd Edition, Wiley Interscience, New York (1981).

Received on 20-11-2015 Accepted on 12-12-2015 Published on 18-12-2015